ORIGINAL ARTICLE
DOI: 10.5433/1679-0375.2022v43n2p199

Bench X-ray microtomography of saline solution/oil injected into samples of the Botucatu/Brazil formation

Microcomografia de raios X de bancada aplicada a solução salina/óleo em amostras da formação Botucatu/Brasil

Leonardo Carmezini Marques[1]; Carlos Roberto Appoloni[2]

Abstract

This paper provides a report on the utilization of the X-ray microtomography to obtain images of the internal microstructure of natural sandstone samples from the Botucatu/Brazil Formation. Its primary objective was to identify the different phases of fluids when injected into the samples to evaluate the various phases through grayscale histograms obtained from 2-D images, quantification of fluid phases, and generation of 3-D images of them. The fluids used in the experiments comprised one type of commercial oil, one type of industrial oil, and an water-salt solution. Quantitative results from 2-D and 3-D analyzes are presented and compared to the volume of injected solution and the measured volume. The phase size distributions indicated which pore radii had a more relevant participation in the percolation of fluids through the samples. Projections in conjunction with 2-D images and profiles of average percentages of air-filled pores indicated the occurrence of preferential percolation flow paths. The 2-D images allowed the measurement of the contact angle between the phases present in the sample containing industrial oil. Different measurements taken from the sample containing commercial oil showed capillary effects indicated by the average percentage profiles of air-filled pores in the 2-D images.

Keywords: x-ray microtomography; fluids; microstructure; sandstone.

Resumo

Este trabalho contém os detalhes da utilização da microtomografia de raios X para obtenção de imagens da microestrutura interna de amostras de arenito da Formação Botucatu/Brasil. O principal objetivo foi identificar diferentes fases de fluidos quando injetadas na amostra para avaliar as diferentes fases através de histogramas de tons de cinza obtidos das imagens 2D, quantificar fases de fluidos e gerar imagens 3D da região escaneada. Os fluidos utilizados nos experimentos foram: um óleo comercial, um óleo industrial e solução água-sal. Resultados quantitativos das análises 2D e 3D são apresentados e comparados com o volume de solução injetado. As distribuições de tamanho de fase indicaram quais raios de poro foram mais relevantes para a percolação de fluidos através da amostra. A análise das projeções e das imagens 2D, juntamente os perfis de porcentagem média de ar nos poros indicaram a ocorrência de caminhos preferenciais de percolação. As imagens 2D permitiram a medida do ângulo de contato entre as fases presentes na amostra contendo óleo industrial. Perfis de porcentagem média de ar nos poros, obtidos com as imagens 2D de diferentes medidas da amostra contendo óleo comercial, mostraram efeitos de capilaridade ocorrendo temporalmente.

Palavras-chave: microtomografia de raios x; fluidos; microestrutura; arenito.

[1] Prof. Dr., IFPR, Londrina, Paraná, Brazil, E-mail: leonardo.carmezini@ifpr.edu.br
[2] Prof. Dr., Dept. Physics, Applaied Nuclear Physics Group, UEL, PR, Brazil, E-mail: appoloni@uel.br

Introduction

Petroleum continues to be an extremely important source of energy, and the search for new wells to meet the growing energy demand is continuous. However, oil extraction becomes increasingly difficult since newly discovered oil reserves lie in regions and conditions of restricted access. An example of this are the oil basins found in the pre-salt areas. The current circumstances demand a relentless pursuit of improved methodologies for the evaluation of the storage capacity and extraction of oil from the new wells, coupled with stringent efforts made to recover remaining oil still trapped in old wells (PETROBRAS, 2019). The petroleum industry makes an extensive use of flooding experiments to model the performance of the reservoir during the processes involved in the extraction of oil (VINEGAR; WELLINGTON, 1987).

The petroleum industry is not the only area interested in the development of knowledge on fluid percolation processes in reservoir samples. The Botucatu formation composes Brazilian main groundwater reservoir, the Guarani aquifer. Main composition of that sandstone rock formation is quartz and clay (CARDOSO; BALABAN, 2015; COSTA *et al.*, 2020; FAGUNDES; ZUQUETTE, 2011). Complementarily, according to a recent study of Costa *et al.* (2020), the Botucatu sandstone is mainly composed of quartz (77%) and clay minerals (15%). Preservation of the groundwater is directly linked to the significant spillage of liquids on the soil surface due to various human activities (FAGUNDES; ZUQUETTE, 2011; ZUQUETTE; PALMA; PEJON, 2006). These incidents generate the trapping of portions of the contaminants in the ground, which are gradually dumped into the groundwater. The process of trapping and releasing contaminant globules depends on how the different types of fluids divide the pore space and which are the effects of capillary forces on the porous medium (BROWN *et al.*, 2014; GOLDSTEIN; PRASHER; GHOSHAL, 2007; WILDENSCHILD; CULLIGAN; CHRISTENSEN, 2004; WILDENSCHILD; HOPMANS, 2005).

The fluid distribution and wettability determine properties, such as capillary pressure, relative permeability, residual saturation, and resistivity index (KUMAR *et al.*, 2009). All these facts underscore the importance of advanced knowledge of the behavior of fluids when in a given porous matrix. X-ray microtomography is a non-destructive methodology that can be used for the direct imaging of fluid distribution at a pore scale (FERNANDES; APPOLONI; FERNANDES, 2019; KUMAR *et al.*, 2009; PAK *et al.*, 2015). This technique was originated in 1972 with medical radiography (VINEGAR; WELLINGTON, 1987). It is based on the absorption of an inhomogeneous X-ray beam transmitted in a particular direction of the sample, generating a linear attenuation coefficient map computationally converted into a digital image, called projection (KAK; SLANEY, 2001; MOREIRA *et al.*, 2012). A reconstruction algorithm utilizes several projections, each of which is taken in a given direction of the sample, to generate 2-D cross-sectional images of the scanned volume. The 2-D model is used for 3-D reconstructions of part or the entire scanned volume (KAK; SLANEY, 2001).

Microtomography-based techniques enable the measurements of fluid/reservoir properties, among which are relative permeability, dispersion, trapped oil saturation, mobility control, and wetting (VINEGAR; WELLINGTON, 1987; PAK *et al.*, 2015). Furthermore, it permits the acquisition of rock microstructural features, such as porosity, size distribution phases, and the investigation of irregularities present in the three-dimensional volume scanned (FERNANDES; APPOLONI; FERNANDES, 2019; RATTANASAK; KENDALL, 2005).

This study aimed to perform saline solution/oil intrusion in sandstone samples from the Botucatu Formation and determine the optimal treatment, indicating used scanning conditions, to distinguish among the different solid, liquid and gaseous phases using X-ray microtomography, identifying some characteristics of the porous environment before and after fluid injection.

Materials and methods

Fluids

One type of fluid was introduced into the sample in each experiment: a solution of water-salt-potassium iodide, water-salt-barium chloride hydrate, oil with SAE 20w50 sold by Petrobras Distribuidora SA, or industrial oil with a density of 0.97 g/cm^3, supplied by CENPES/PETROBRAS.

Water-salt solution was used because the petroleum industry uses water injection to keep the pressure inside the reservoir and allow the recovery of additional amounts of crude oil (OLIVEIRA; SANTELLI; CASSELLA, 2008). However, a solution composed just of salt and water does not provide enough visual contrast to tomography images to discriminate brine from other analyzed phases.

Therefore, potassium iodide or hydrated barium chloride were used as dopants. Iodine and barium have the ability to increase the absorption of X-rays by the solution. Table 1 shows the compositions of each solution tested for the experiments and the percentages (%) of the compounds water (H_2O), sodium chloride (NaCl), potassium iodide (KI) and hydrataded barium chloride ($BaCl_2.2H_2O$) used to obtain each solution.

Table 1 – Solutions used in the experiments.

Nomenclature	H_2O (%)	NaCl (%)	KI (%)	$BaCl_2.2H_2O$ (%)
Solution 1	70.0	17.0	13.0	-
Solution 2	72.0	18.0	10.0	-
Solution 3	73.3	13.3	-	13.3

Source: The authors.

From the compositions of each solution tested for the experiments, Figure 1 was obtained.

Figure 1 – Theoretical linear X-ray attenuation coefficients (μ) versus energy of saline solutions, the main component of the sample (SiO_2) and the dopants used versus energy.

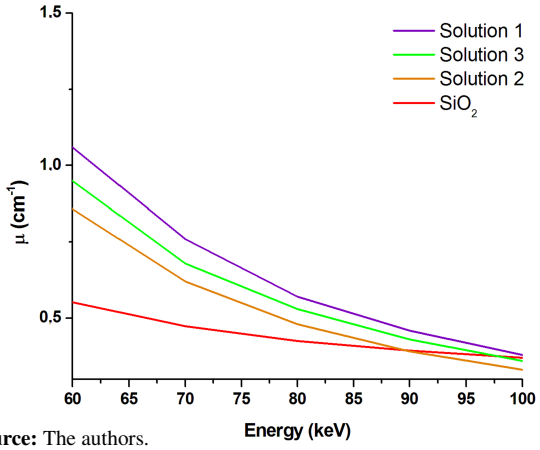

Source: The authors.

Note the graph in Figure 1 reveals that solution 1 presents linear attenuation coefficients values higher than the other compounds, including the sample itself, for energies between 60-100 keV. This means that the X-rays are more absorbed by solution 1 than the others and the sample itself, increasing the probability of solution 1 be distinguishable in the tomography image by means of a grayscale interval compared to the other phases. Despite having a linear attenuation coefficient very close to the main component of the sample for energies between 95 and 100 keV, the solution 3 was also analyzed to test its performance as dopant, since its chemical composition is quite different from other solutions.

Linear attenuation coefficients values presents in Figure 1 were performed with XCOM software (BERGER; HUBBELL, 1987; GERWARD *et al.*, 2001).

Rocks

A sample of nylon thread was used to test the X-ray microtomographic techique, where a complete description of this experiment and results can be seen in Marques, Appoloni and Fernandes (2011). Six sandstone samples from the Botucatu/Brazil formation, denotad for ARNi, i=1,...,6, provided by the Department of Geosciences (DGEO) from State University of Londrina were analysed, as shown in Table 2.

Table 2 – Samples nomenclature and fluids used in the tests.

Sample	Fluid injected
ARN1	Solution 1
ARN2	Solution 1
ARN3	Solution 2
ARN4	Solution 3
ARN5	Commercial oil
ARN6	Industrial oil

Source: The authors.

As can be seen in Table 2, four samples were used in the experiments with saline solutions, ARNi, i=1,...,4, and two with the oils, ARN5 and ARN6.

Equipment and Softwares

Two laboratories provided their devices for the experiments: the Petrobras Research Center (CENPES/PETROBRAS), Rio de Janeiro, RJ, and the Laboratory for Analysis of Minerals and Rocks (LAMIR), Federal University of Paraná (UFPR), Curitiba, PR.

The two microtomography scanners were the Skyscan model 1172, of Bruker corporation. This device works with micro-focus X-ray tube (W anode and 5 μm spot size) operating at applied tension from 20 to 100 kV, with maximum power of 10 W. Its detector is a CCD camera. This set can differentiate between details smaller than 1 μm.

Some specific software tools were used, where the "NRecon" reconstructs 2-D images based on acquired projections employing the most widely used reconstruction technique called filtered back projection (KETCHAM; CARLSON, 2001). For image analysis, two software tools were used: the "Imago" software helped with the selection of the appropriate gray level for image segmentation; and the gray level was applied to the "CTAn" software

for results obtained from the 2-D images and/or volume (3-D). The software "CTAn" was also used to generate 3-D images displayed on the "CTvol" software. The Data Acquisition software for the Skyscan equipment was also utilized. Among the mentioned software tools, only the "Imago" one is not part of the Skyscan pack. This software was developed at the Laboratory of Porous Media and Thermophysical Properties (LMPT), Department of Mechanical Engineering, Federal University of Santa Catarina in association with Engineering Simulation and Scientific Software (ESSS) and Petrobras.

Procedures

First, measurements with sandstone dry samples were accomplished and then measured again after infiltration with one type of fluid. Figure 2 presents Botucatu/Brazil sandstone, aluminum sample holder photos and bonding scheme positioning of the sample within the teflon sleeve, where teflon sleeve with 8 mm outer diameter and 1 mm wall thickness and 6 mm diameter Botucatu sandstone sample, left in Figure 2(a). Figure 2(b) shown the bonding scheme positioning of the sample within the teflon sleeve with space for deposition of fluid and indication of vacuum application, middle. Finally, in Figure 2(c), there is the aluminum sample holder with 8 mm internal diameter and 1 mm wall thickness.

Figure 2 – (a) Teflon sleeve (left) and Botucatu/Brazil sandstone sample (right); (b) bonding scheme positioning of the sample within the teflon sleeve with space for deposition of fluid and indication of vacuum application; and (c) aluminum sample holder.

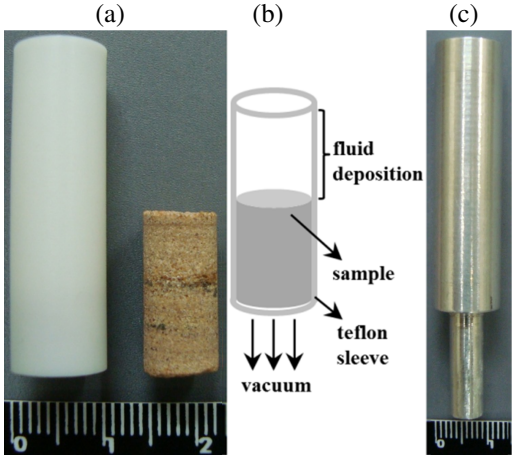

Source: The authors.

Figure 2(a) shows a picture of one of the sandstone samples utilized in the experiment taken from one of the original rocks next to a Teflon sleeve. The sample was placed within the sleeve using resin so that only the top and back sides were available for fluid inlet and outlet, besides an opening at one of the extremities allowing fluid to be deposited in the top part, as indicated in Figure 2(b). The back side of the set was vacuum-applied to facilitate fluid penetration. The application of vacuum was interrupted whenever the sample surface on which the solution was applied showed wetting signals. After this stage, with the sample already positioned within the Teflon sleeve was introduced into an aluminum sample holder and the set was imaged. An exception was used for the ARN6 sample. The sample was allowed to rest for approximately 15 hours before being imaged. Figure 2(c) shows the aluminum sample holder designed to maintain the samples with fluid during the scanning. Sleeve and sample holder walls acted as a filter to absorb X-ray photons of lower energy, which could cause beam hardening effects on the images (VINEGAR; WELLINGTON, 1987).

All samples were measured with a spatial resolution of approximately 4.8 μm/pixel and voltages ranging from 60 to 90 kV applied to the X-ray tube. The measurements of ARN1 and ARN2 samples were taken using an exposure time of 5015 ms and 180° rotation. For the measurements of the remaining samples, the exposure time of 2125 ms and 360° rotation were used. The analyses of microstructural characterization start with the segmentation of the 2-D grayscale images, by the selection of a threshold point in the grayscale histogram of each image. The purpose of binarization is to separate the phase of interest to be anayzed (MOREIRA *et al.*, 2012; SAETRE; TJUGUM, 2014; SEZGIN; SANKUR, 2004).

Results and discussions

Solutions analyses

In general, the results obtained are nearly the same for all samples containing the various solution types. No solution stood out within the porous volume, where the pores are black, as can be seen in Figure 3. Dry sandstone samples, Figure 3(a)-(d), and infiltrated sandstone samples, Figure 3(e)-(h), with the solutions, ARNi, i=1,⋯,4, from left to right, respectively. However, the solution can be identified in the section corresponding to the infiltrated ARN4 sample, where the solution light gray. It appears on the edge of the image, between the teflon sleeve and the sandstone where sandstone is gray.

Figure 3 – 2-D images for the ARNi samples, i=1,⋯,4, from left to right, respectively. Sections of the: (a)-(d) dry samples and (e)-(h) infiltrated samples. The pores are black, the sandstone is gray and the solution is light gray.

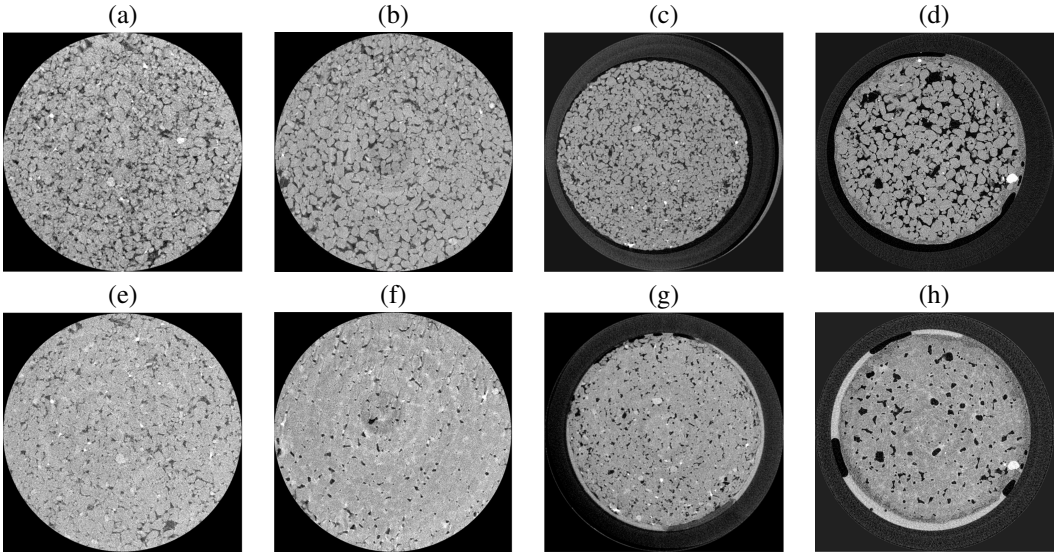

Source: The authors.

Figure 4 shows examples of projections obtained for the ARN4 sample, in which solution 3 was injected. This sandstone sample has its results better detailed in this article because its porosity and phase size distribution resulted in more didactic images for discussions and because it was possible to gravimetrically quantify the injected liquid volume for comparison with the results obtained by microtomography.

Figure 4 – Projections obtained for the ARN4 sample: (a) dry sample and (b) sample with solution 3.

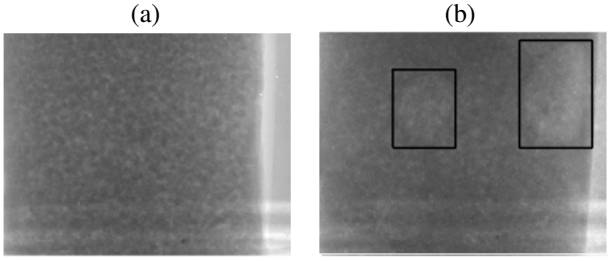

Source: The authors.

In Figure 4(a), the sample is dry while in Figure 4(b) the sample contains the solution 3. General acquisition parameters were: spatial resolution of 4.9 μm, angular step of 0.40º, 360º rotation, 4 frames and 1336 x 2000 pixels on the CCD camera; the specific parameters were: 80 kV applied voltage, 2000 ms exposure time for the dried sample and 90 kV and 2600 ms for the sample containing the solution. The highlighted areas in Figure 4(b) evidence that in this case, the solution could not access those areas because the capillary barriers have not been overcome, thus the fluid took preferential paths to percolate the sample. Similar results were found by Bultreys, Boever and Cnudde (2016).

Figure 5 shows reconstructed 2-D images from the ARN4 sample. Figures 5(a) and 5(c) are examples of grayscale images samples both in dry condition and containing the solution, respectively. Figures 5(b) and 5(d) show the same binarized images for analysis. The $BaCl_2.2H_2O$ solution did not present a visible characteristic grayscale interval in the microtomography images. However, the filling of the porous phase was clearly detectable.

Figure 5 – 2-D images for the ARN4 sample: (a) image of section 285 for the dry sample; (b) binarized image of section 285 for the dry sample; (c) image of section 300 for sample which was infiltrated; and (d) binarized image of section 300 for the sample which was infiltrated.

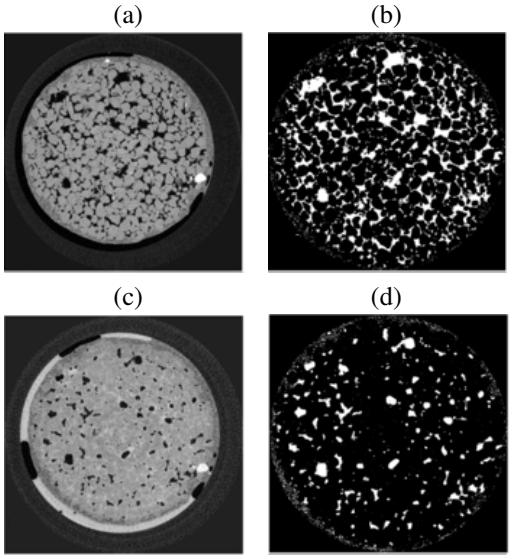

Source: The authors.

Based on 2-D images, see Figure 5, one can assume the probable occurrence of some reaction between the compounds found in the solution and components of the sample itself, for example, barium chloride hydrate may have undergone an adsorption process with clay that possibly exists in the sample. Similarly, the water-salt solution containing potassium iodide was not characterized by a clear grayscale interval, and the 2-D images showed a behavior similar to that of the sample images containing the solution doped with barium chloride hydrate. Therefore, the dopant compound may have reacted with the compounds present in the sample. Other authors have also observed this phenomenon (RAO; SIVACHIDAMBARAM, 2013; RIEBE; DULTZ; BUNNENBERG, 2005) and have even used this interaction to achieve their research objectives (FOGDEN *et al.*, 2014).

Figure 6 shows the profiles of the average percentages of pores filled with air obtained for the sample ARN4 with Imago software. Profiles of the mean percentages of airspaces for each 2-D image of the of the ARN4 samples dry and containing the solution (wet) are illustrated in red and green color, respectively.

Figure 6 – Profiles of the average percentages of air spaces for each 2-D image of the ARN4 sample: dray, red color, and containing the solution (wet), green color.

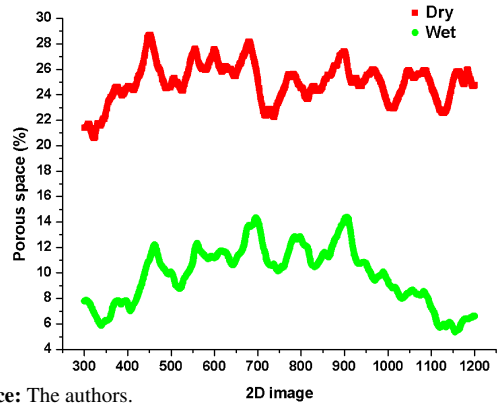

Source: The authors.

Note that the profile obtained for the sample containing the solution, illustrated in Figure 6, green color, showed that pores with higher percentages of air tended to be found among the 2-D images for slices from 428 to 1020. Table 3 shows the sample volume and the volume of liquid that was injected. On the other hand, Table 4 shows summarize the results with the total volume values obtained through 2-D and 3-D analysis for the sample ARN4, but also for the other samples. Regarding the analyzed volume of this sample - 113 mm^3, the average percentage values of the volume filled with air were 25.0 (3.0)% and 9.8 (4.5)% before and after the injection of the solution, respectively. These results show a decrease of 61% or 17 (2) mm^3 in fluid intrusion in the scanned volume. The deviations presented between parentheses were calculated considering the Gaussian distribution with a 95% confidence interval.

Table 3 – ARN4 sample volume and injected liquid volume.

Sample volume (mm^3)	Injected volume (mm^3)
765 (11)	163 (13)

Source: The authors.

Table 4 – Porosity before and after liquid injection, obtained volume of liquid.

		Dry (%)	Solution (%)	Achieved volume (mm^3)
ARN1	2-D	7.2 (1.0)	1.7 (0.6)	10 (2)
	3-D	6.4 (1.4)	1.3 (0.4)	10 (3)
ARN2	2-D	7.2 (3.1)	2.3 (0.9)	9 (3)
	3-D	6.3 (1.7)	2.0 (0.2)	6 (4)
ARN3	2-D	14.3 (7.5)	6.0 (2.7)	11 (2)
	3-D	13.1 (2.2)	5.5 (0.2)	15 (3)
ARN4	2-D	25.0 (3.0)	9.8 (4.5)	17 (2)
	3-D	24.7 (0.6)	9.6 (0.2) 1	7 (1)

Source: The authors.

The volume of liquid found through the 3-D analysis was 17 (1) mm^3. The volume imaged by 3-D method corresponds to the same volume analyzed by 2-D method - 113 mm^3. The volume of the injected solution was 163 (13) mm^3 in a total of 765 (11) mm^3 of the sample. Taking into account the deviations, the liquid volumes obtained by the 2-D and 3-D analyzes are, respectively, 2% and 3% smaller than the volume of liquid injected into the sample. This difference between the values may have resulted from the difficulty in accurately obtaining the total volume of each sample due to its irregular shape. Furthermore, the possible reactions between the compounds existing in both the solutions and the sample would result in a lower quantification of liquid using X-ray microtomography. The analyzed volume the samples ARN1, ARN2 and ARN3 were 186, 173 and 138 mm^3, respectively.

Figure 7 shows the phase size distribution in ARN4 sample dry and containing the solution (wet). The size diversity of volume with air combined with their frequency of occurrence makes this sample the one with the highest average total open space. Through the phase size distribution, it is possible to see that the wet sample revealed a decrease in the relative frequency of volume with air with radii between 9.8 μm and 34.3 μm, which means that in

this case these pores were the primary responsible for the fluid percolation throughout the sample.

Figure 7 – Phase size distribution of air for the ARN4 sample before and after the injection of the solution in the porous space.

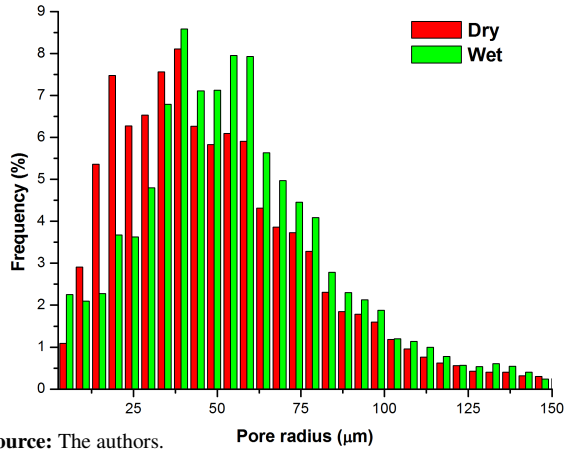

Source: The authors.

The other samples exhibited similar results, except the ARN1 sample, which presented an open space value much lower than the others, as it corresponds to only 10% of the open space of the ARN4 sample, the most porous. Possibly, the majority of the pores with radii smaller than 4.8μm (which is the spatial resolution used) are closed pores and thus do not participate in the fluid percolation (SI *et al.*, 2019). The ARN1 sample presented a decrease in the relative frequency of air spaces with radii equal to or greater than 19.3μm, as shown in Figure 8.

Figure 8 – Phase size distribution of air for the ARN1 sample before and after the presence of the solution (wet) in the porous space.

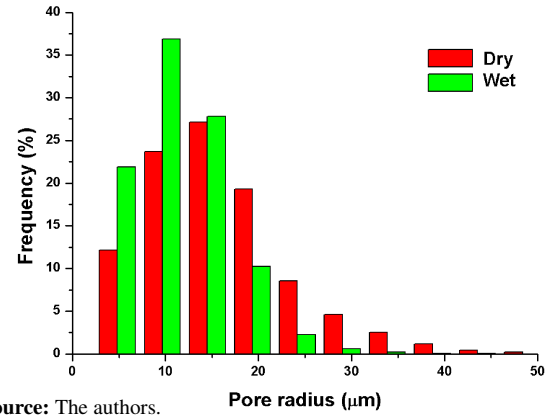

Source: The authors.

Figure 9 shows the reconstructed 3-D images of the ARN4 sample, dry in Figure 9(a) and impregnated with solution 3 in Figure 9(b). Both images have a diameter of 2000 μm and were prepared based on 2-D image intervals from section 300 to 700.

The porous space filled with air is red color while the solid phase appears in translucid. Figure 9(b) has spaces with large volumes, which confirms the observations recorded through the phase size distributions.

Figure 9 – 3-D image for the ARN4 sample highlighting the porous environment filled with air, red color: (a) shows the dry sample and (b) the sample percolated with the solution.

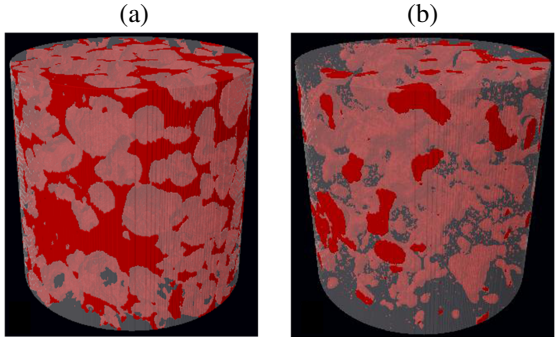

Source: The authors.

Experiment with industrial oil

The ARN6 sample was imaged before and after industrial oil injection. The 2-D images shown in Figure 10 correspond to approximately the same position in the sample and show a change in the contrast corresponding to the porous region of the sample containing oil, Figure 10(b), compared to the dry sample, Figure 10(a). Although a grayscale interval characteristic of this phase is not visually detectable, it is possible to observe the presence of oil in the porous environment.

Figure 10 – 2-D images for the ARN6 sample. (a) Dry sample image of section 259; (b) Industrial oil image of section 279.

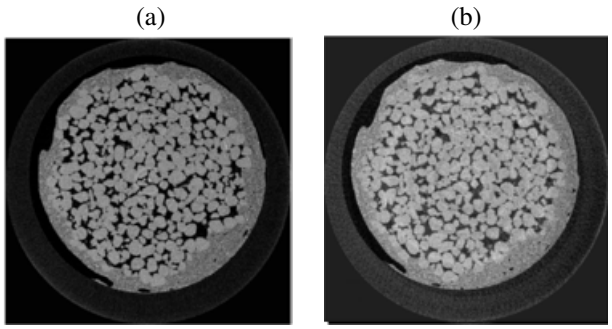

Source: The authors.

Figure 11 can be used to corroborate the statement, as it presents details of 2-D images in Figure 10, as well as their grayscale histograms.

Figure 11 – (a) Dry sample detail of the grayscale threshold selection window for binarization and grayscale histogram with the respective binarization thresholds chosen, at the Imago software, for the section 259 of the image and (b) industrial oil sample for the image 279. Both images are binarized / merged. Examples of contact angles between the solid phase and air are indicated for the interface among air-solid-oil phases.

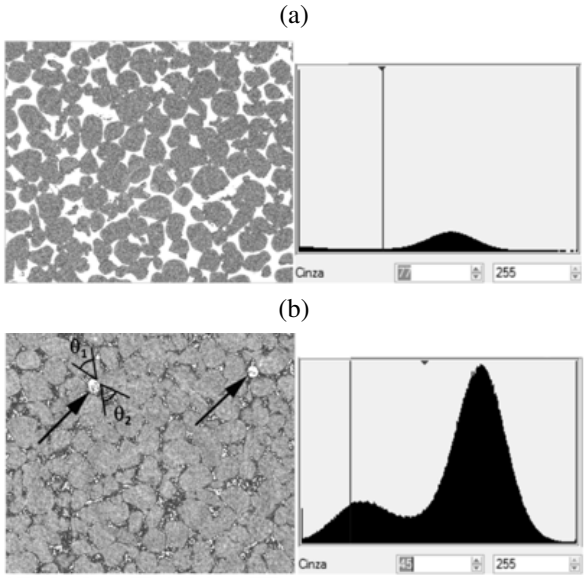

Source: The authors.

One can observe the formation of air bubbles as highlighted by arrows in Figure 11(b). The angular separation between the solid and air phases (angles θ_1 and θ_2) was qualitative estimated with CTAn software tool. The values found for the angles θ_1 and θ_2 are 28.5 (2.3)° and 33.8 (4.3)°, respectively. In this sandstone-oil-air interface zone, we can observe that oil is the wetting phase, and air is the non-wetting phase relative to the sandstone since the contact angle between the air and sandstone systems is smaller than 90° (BEAR, 1988; BROWN *et al.*, 2014; ZENG; LI; FEN-CHONG, 2012). The deviations shown were calculated considering the Student's t distribution with 95% confidence interval for a set of 10 measurements taken at each angle. The histogram in Figure 11(b) provides a better definition of the peak corresponding to the levels of gray representative of the solid phase. The grayscale threshold for the sample containing industrial oil was chosen to identify the outline of the air bubbles. There are levels of gray shared by both the oil phase and the noise inherent in the measurement sensor.

Figure 12 shows the profiles of spaces filled with air in ARN6 sample. The percentage values of the air phase decrease, even if there is not a perfect definition of the oil phase.

Figure 12 – Profiles of the average percentages of volumes with air of each 2-D image for the ARN6 sample: dried, red color, and after percolation with of industrial oil, green color.

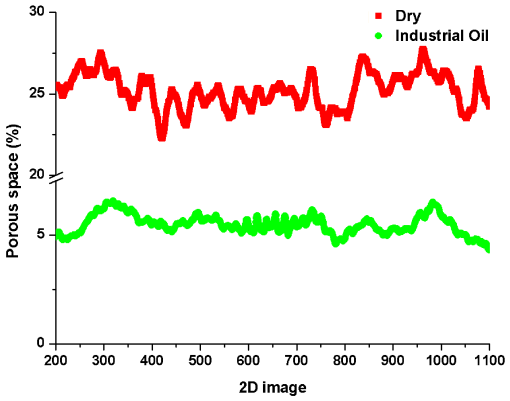

Source: The authors.

Figure 13 shows four reconstructions of the ARN6 sample. They were generated using the same interval of 400 slices of the sample.

Figure 13 – 3-D images for the ARN6 sample: (a) porous region of the dry sample, (b) the solid phase to the infiltrated sample with oil, (c) air spaces with the sample infiltrated with oil and (d) spaces with air and oil with the sample containing oil. The images are 2000 µm in diameter and 1965 µm height.

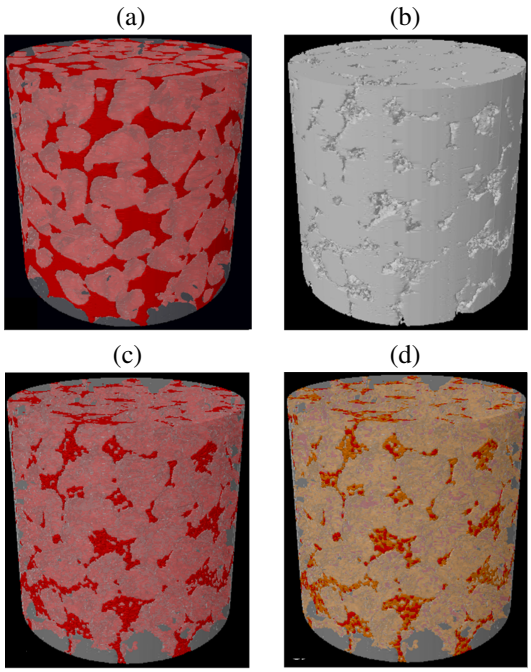

Source: The authors.

Figure 13(a) was constructed using the 3-D image of the solid phase with grayscale intervals from 72-255 overlapped with the 3-D image of the porous spaces with grayscale intervals from 0-71, both acquired from the 2-D images with the measurements taken from the dry sample.

The images, Figures 13(b)-(d), were prepared based on the 2-D images measured with the sample containing oil. Figure 13(b) shows a reconstruction of the solid phase and corresponds to the grayscale interval from 75 to 255. Figure 13(c) displays the overlap of the previous 3-D image with the reconstruction of the air phase, whose grayscale values range from 0-41. Finally, Figure 13(d) corresponds to the overlapping of the two 3-D images used in the image Figure 13(c) with the reconstruction of the oil phase, whose grayscale values range from 42 to 74. Figures 13(c) and 13(d) complement each other. Only the 3-D image of the air phase would mark the relevance of the oil phase occurrence.

Experiment with commercial oil

As evidenced in the case of the experience with glass balls as matrix for percolation (MARQUES; APPOLONI, 2015), the industrial oil revealed to be more attenuating than the commercial oil. However, it is worth presenting a result related to the latter type of oil. Figure 14 shows the profiles of the average percentages of pores filled with air in each 2-D image of the ARN5 sample scanned volume. Red, green and blue colors correspond to the dry sample, to the sample containing commercial oil measured at 80 kV, and to the sample with the same oil, but measured at 60 kV, respectively. The latter two measurements were performed consecutively. The objective was to improve the contrast between the different phases present in the sample.

Figure 14 – Profiles of the average percentages of volumes with air of each 2-D image for the ARN5 sample dried, red color, with percolation of commercial oil and measured at 80 kV, green color, and measured at 60 kV, blue color.

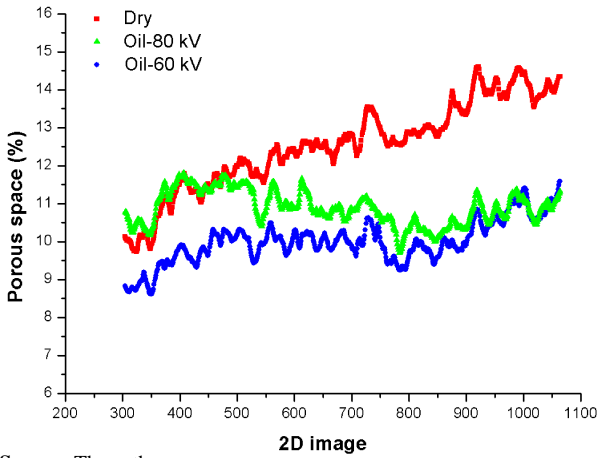

Source: The authors.

The right side of Figure 14 shows the results obtained from the top of the sample, which is the side through which the fluid was injected. The images closer to the sample bottom show a coincidence between the average percentage values of pores filled with air in relation to the measurements taken with the dry sample and oil (80 kV). This fact occurs from the cross-section image number 304 (first) to approximately the cross section image number 485, meaning that the oil had not yet performed percolation throughout the vertical extent of the sample. Notwithstanding, there is also a coincidence between the average percentage values of pores with air and the images near the top of the sample in relation to the two measurements with the sample containing oil. In this case, the coincidence is seen from approximately the cross-sectional image 901 to 1064 (last image). This coincidence means that the oil continued performing percolation during the second measurement accomplished with the sample in Figure 14 (with oil and at 80 kV), reaching the bottom of the sample before the last measurement period (with oil and at 60 kV). As the total time of each measurement was 3 hours and 13 minutes, we can infer that the fluid took less than 6 hours and 26 minutes to percolate, by capillary action, throughout the vertical direction of the sample.

The commercial oil, despite being less attenuating, provided enough attenuation of the X-ray beam to differentiate the profiles of the average percentages of volumes with air, as seen in the case of industrial oil, see Figure 12.

Conclusions

The results obtained support qualitatively that the employment of the X-ray microtomography methodology, using a bench-top equipment, in such type of work requires the selection or processing of samples, and/or doping of liquids utilized to acquire adequate 2-D and 3-D images.

Actually, results obtained are nearly the same for all samples containing the various solution types. More striking results were provided by sample with a greater volume of porous space. This is the case of ARN4 sample in which it was possible to measure the solution 3 volume injected.

The phase size distribution shows a satisfactory result for sandstone samples before and after the injection of the solution in the sample. These graphs indicate the most relevant pore radii interval for fluid percolation in the sample.

In general, smaller pore radii participated in the percolation. This tendency was inverted only in the ARN1 sample, which exhibits open porosity values much lower than the others (only 10% of the open porosity values of the ARN4 sample, which is the more porous sample). The results for ARN 1 indicate that the phase distribution must be taken into account when studies are carried out to check pores relevant for fluid percolation.

The percentage profiles of pores filled with air obtained from the ARN5 and ARN6 samples indicated the presence of the oil phase in the porous region, even without adding a dopant to this fluid.

Acknowledgments

Our best thanks to CENPES/PETROBRAS, LAMIR/UFPR and LARX/UEL laboratories for the measurements taken in their facilities, professor Dr. Celso Peres Fernandes and LMPT/UFSC laboratory for granting permission for the utilization of IMAGO software, and CNPq for fostering our research.

References

BEAR, J. *Dynamics of fluids in porous media, x ed.* Dover: Dover Publications, 1988.

BERGER, M. J.; HUBBELL, J. H. *XCOM*: photon cross sections on a personal computer. Washington: Departament of Commerce, 1987. DOI: http://dx.doi.org/10.2172/6016002.

BROWN, K..; SCHLÜTER, S.; SHEPPARD, A.; WILDESCHILD, D. On the challenges of measuring interfacial characteristics of three-phase fluid flow with x-ray microtomography. *Journal of Microscopy*, Oxford, v. 253, p. 171-182, 2014. DOI: https://doi.org/10.1111/jmi.12106.

BULTREYS, T.; BOEVER, W. D.; CNUDDE, V. Imaging and image-based fluid transport modeling at the pore scale in geological materials: A practical introduction to the current state-of-the-art. *Earth-Science Reviews*, Amsterdam, v. 155, p. 93-128, 2016. DOI: http://dx.doi.org/10.1016/j.earscirev.2016.02.001.

CARDOSO, O. R.; BALABAN, R. C. Comparative study between Botucatu and Berea sandstone properties. *Journal of South American Earth Sciences*, Oxford, v. 62, p. 58-69, 2015. DOI: http://dx.doi.org/10.1016/j.jsames.2015.04.004.

COSTA, A. A.; TRIVEDI, J.; SOARES, J.; ROCHA, P.; COSTA, G.; EMBIRUÇU, M. An experimental evaluation of low salinity water mechanisms in a typical Brazilian sandstone and light crude oil with low acid/basic number. *Fuel*, London, v. 273, p. 1-18, 2020. DOI: https://doi.org/10.1016/j.fuel.2020.117694.

FAGUNDES, J. R. T.; ZUQUETTE, L. V. Sorption behavior of the sandy residual unconsolidated material from the sandstones of the Botucatu Formation, the mais aquifer of Brazil. *Environmental Earth Science*, Berlin, v. 62, p. 831-845, 2011. DOI: http://doi.org/10.1007/s12665-010-0570-y.

FERNANDES, J. S.; APPOLONI, C. R.; FERNANDES, C. P. Siltstone and sandstone pore space by X-ray microtomography. *Soils and Rocks*, São Paulo, v. 42, n. 3, p. 281-288, 2019. DOI: https://doi.org/10.28927/SR.423281.

FOGDEN, A.; MIDDLETON, J.; MCKAY, T.; LATHAM, S.; MARATHE, R.; TURNER, M.; SHEPPARD, A.; HOWARD, J. J.; LANE, F. D. 3D mapping of pore and organic matter distributions in unconventional reservoir utilizing a digital rocks approach. *In*: INTERNATIONAL SYMPOSIUM, SOCIETY OF CORE ANALYSTS AVIGNON, 2014, France. *Proceedings* [. . .]. France: [*S. l.*], 2014. p. 1-12.

GERWARD, L.; GUILBERT, N.; JENSEN, K. B.; LEVRING, H. X-ray absorption in matter. Reengineering XCOM. *Radiation Physics and Chemistry*, Oxford, v. 60, n. 1/2, p. 23-24, 2001. DOI: https://doi.org/10.1016/S0969-806X(00)00324-8.

GOLDSTEIN, L.; PRASHER, S. O.; GHOSHAL, S. Three-dimensional visualization and quantification of non-aqueous phase liquid volumes in natural porous media using a medical X-ray Computed Tomography scanner. *Journal of Contaminant Hydrology*, Amsterdam, v. 93, p. 96-110, 2007. DOI: http://dx.doi.org/10.1016/j.jconhyd.2007.01.013.

KAK, A. C.; SLANEY, M. *Principles of computerized tomographic imaging*. New York: IEEE Press, 2001. DOI: https://doi.org/10.1137/1.9780898719277.

KETCHAM, R. A.; CARLSON, W. D. Acquisition, optimization and interpretation of X-ray computed tomographic imagery: applications to the geosciences. *Computers & Geosciences*, Oxford, v. 27, p. 381-400, 2001. DOI: http://dx.doi.org/10.1016/S0098-3004(00)00116-3.

KUMAR, M.; SENDEN, T.; KNACKSTEDT, M.; LATHAM, S.; PINCZEWSKI, V.; SOK, R. M.; SHEPPARD, A. P.; Turner, M. L. Imaging of pore scale distribution of fluids and Wettability. *Petrophysics Journal*, Houston, v. 4, p. 311-321, 2009. DOI: http://hdl.handle.net/1885/52974.

MARQUES, L. C.; APPOLONI, C. R.; FERNANDES, C. P. Porosity study of synthetic sandstones by non-destructive nuclear techniques. *Materials Research*, New York, v. 14, n. 3, p. 1-9, 2011. DOI: http://dx.doi.org/10.1590/S1516-14392011005000048.

MARQUES, L. C.; APPOLONI, C. R. Quantification of fluids in a glass-bead matrix using X-ray microtomography. *Micron*, New York, v. 75, p. 35-43, 2015. DOI: http://dx.doi.org/10.1016/j.micron.2015.03.001.

MOREIRA, A. C.; APPOLONI, C. R.; MANTOVANI, I. F.; FERNANDES, J. S.; MARQUES, L. C.;NAGATA, R.; FERNANDES, C. P. Effects of manual threshold setting on image analysis results of a sandstone sample structural characterization by X-ray microtomography. *Applied Radiationand Isotopes*, Oxford, v. 70, p. 937-941, 2012. DOI: http://dx.doi.org/10.1016/j.apradiso.2012.03.001.

OLIVEIRA, E. P.; SANTELLI, R. E.; CASSELLA, R. J. Combined use of Pd and HF as chemical modifiers for the determination of total chromium in produced waters from petroleum exploration by ET AAS. *Microchemical Journa*l, New York, v. 89, p. 116-122, 2008. DOI: http://dx.doi.org/10.1016/j.microc.2008.01.002.

PAK, T.; BUTLER, I. B.; GEIGER, S.; VANDIJKE, M. I. J.; SORBIE, K. S. Doplet fragmentation: 3D imaging of a previously unidentified pore-scale process during multiphase flow in porous media. *PNAS*, [Oxford], v. 112, n. 7, p. 1947-1952, 2015. DOI: www.pnas.org/lookup/suppl/doi:10.1073/pnas.1420202112/-/DCSupplemental.

PETROBRAS. *Tecnologia e Pesquisa*. Rio de Janeiro: Petrobras, 2019. Available from: <https://petrobras.com.br/pt/nossas-atividades/areas-de-atuacao/exploracao-e-producao-de-petroleo-e-gas/pre-sal/>. Access in: Dec. 2022.

RAO, S. M.; SIVACHIDAMBARAM, S. Characterization and iodide adsorption behavior of HDPY + modified bentonite. *Environmental Earth Sciences*, Berlin, v. 68, p. 559-566, 2013. DOI: http://dx.doi.org/10.1007/s12665-012-1759-z.

RATTANASAK, U.; KENDALL, K.. Pore structure of cement/pozzolan composites by X-ray microtomography. *Cement and Concrete Research*, Oxford, v. 35, p. 637-640, 2005. DOI: http://dx.doi.org/10.1016/j.cemconres.2004.04.022.

RIEBE, B.; DULTZ, S.; BUNNENBERG, C. Temperature effects on iodine adsorption on organo-clay minerals I. Influence of pretreatment and adsorption temperature. *Applied Clay Science*, Amsterdam, v. 28, p. 9-16, 2005. DOI: http://dx.doi.org/10.1016/j.clay.2004.01.004.

SAETRE, C.; TJUGUM, S. Tomographic segmentation in multiphase flow measurement. *Radiation Physics and Chemestry*, Oxford, v. 95, p. 420-423, 2014. DOI: http://dx.doi.org/10.1016/j.radphyschem.2013.03.025.

SEZGIN, M.; SANKUR, B. Survey over image thresholding techniques and quantitative performance evaluation. *Journal of Electronic Imaging*, Bellingham, v. 13, n. 1, p. 146-165, 2004. DOI: http://dx.doi.org/10.1117/1.1631316.

SI, L.; LI, Z.; KIZIL, M.; CHEN, Z.; YANG, Y.; JI, S. The influence of closed pores on the gas transport and its application in coal mine gas extraction. *Fuel*. London, v. 254, 2019. DOI: https://doi.org/10.1016/j.fuel.2019.06.013.

VINEGAR, H. J.; WELLINGTON, S. L. Tomographic Imaging of Three-Phase Flow Experiments. *The Review of Scientific Instruments*, Woodbury, v. 58, n. 1, p. 96-107, 1987. DOI: http://dx.doi.org/10.1063/1.1139522.

WILDENSCHILD, D.; CULLIGAN, K. A.; CHRISTENSEN, B. S. B. Application of x-ray microtomography to environmental fluid flow. *SPIE Digital Library*, Bellingham, v. 5535, 2004. DOI: http://dx.doi.org/10.1117/12.559056.

WILDENSCHILD, D.; HOPMANS, J. W.; Kent, A. J. R. Quantitative Analysis of Flow Process in a Sand Using Synchrotron-Based X-ray Microtomography. *Vadose Zone Journal*, Madison, v. 4, p. 112-126, 2005. DOI: http://dx.doi.org/10.2113/4.1.112.

ZENG, Q.; LI, K.; FEN-CHONG, T.; DANGLA, P. Analysis of pore structure, contact angle and pore entrapment of blended cement pastes from mercury porosimetry data. *Cement and Concrete Composites*, Amsterdam, v. 34, n. 9, p. 1053-1060, 2012. DOI: http://dx.doi.org/10.1016/j.cemconcomp.2012.06.005.

ZUQUETTE, L. V.; PALMA, J. B.; PEJON, O. J. Initial assessment of the infiltration and overland flow for different rainfall events in land constituted of sandstones of the Botucatu Formation (Guarani Aquifer), State of São Paulo, Brazil. *Environmental Geology*, Heidelberg, v. 50, p. 371-387, 2006. DOI: http://dx.doi.org/10.1007/s00254-006-0216-2.

Received: Oct. 4, 2022
Accepted: Dec. 22, 2022
Published: Dec. 29, 2022